Creep behaviour of single hemp fibres. Part II: Influence of loading level, moisture content and moisture variation.

Violaine Guicheret-Retel[1], Ousseynou Cisse[1], Vincent Placet[1*], Johnny Beaugrand[2,3], Miguel Pernes[2,3], M. Lamine Boubakar[1]

[1] *Department of Applied Mechanics, FEMTO-ST Institute, UMR CNRS 6174,University of Franche-Comté, F-25000 Besançon, France*

[2] *INRA, UMR 614 Fractionnement des AgroRessources et Environnement, F-51100 Reims, France*

[3] *Université de Reims Champagne-Ardenne, UMR614 Fractionnement des AgroRessources et Environnement, F-51100 Reims, France*

* Corresponding author: Email: vincent.placet@univ-fcomte.fr
tel: +33 (0)3 81 66 60 55 - fax: +33 (0)3 81 66 67 00

ABSTRACT

This work investigates the tensile creep behaviour of single hemp fibres under constant and cyclic loading coupled to constant or variable moisture content environment. Results show that the primary creep strain rate of such fibres decreases with increasing stresses, while the secondary creep strain rate increases. Load cycling at an average load higher than constant creep load produces a large additional extra creep strain and an increase of the creep rate. Both primary and secondary creep strain rates increase with increasing moisture content. More creep is also observed in cyclic humidity conditions than in a constant environment at the high-humidity. In agreement with some observations on synthetic fibres, we showed that this accelerated creep is only observed for high moisture cycling rates. This mechanosorptive effect is consistent with sorption-induced stress-gradient explanations proposed in literature.

Key words: hemp fibres / creep / mechanosorptive effect

INTRODUCTION

The first part of this extensive work (Part I) provides the major tendency of the creep behaviour of isolated single hemp fibres under constant climate. Unlike classical glass and carbon fibres, the tensile behaviour of plant-based fibres is highly nonlinear (*1*) and depends strictly on their humidity (*2*). So, the question of the influence of stress and moisture levels on the time-dependent behaviour is of great importance and has to be accurately characterised. The existence of a mechanosorptive (MCS) effect in hemp fibre remains an open query. Indeed, although the MCS effect has been studied since the late 1950s for wood and paper materials (*3*), the topic is highly contentious and there is no widely accepted explanation. Its existence for single fibres is widely debated in the scientific community since negative results have been published (*4-7*). Effectively, the review of literature shows that the conclusions regarding the MCS effect for single fibres are mixed; some fibre exhibit accelerated creep (*8-10*), whereas others seem to resist (*4-6*). According to Haberger *et al*. (*7*) the widespread lack of observance of single-fibre accelerated creep is due to an experimental parameter rather than a fundamental difference in material behaviour. Authors attributed the absence of accelerated creep to an inadequate moisture cycling rate. Habeger *et al*. (*7*) demonstrated experimentally for several hydrophilic fibres, such as Kevlar, lyocell, ramie and nylon 6-6, that the MCS effect happened only because of the choice of humidity cycling parameters. They argue that accelerated creep is a phenomenon consistent with sorption-induced stress-gradient explanations (*7, 11*). The recent results of Lindström *et al*. (*12*) on nanocellulose materials seems to contradict this hypothesis since the MCS creep is not significantly affected by the through-thickness moisture gradient. Authors suggest that the MCS effect in this type of materials could be attributed to the interfibril bonds or possibly to the microfibrils themselves. Others mechanisms and levels of explanation can also be proposed. Dong *et al*. (*8*) pointed out for example the influence of the fibre morphology and more exactly on the microfibril angle (MFA) on the MCS creep. At high microfibril angles (MFA), the MCS effect could be non-existing.

So, the aim of this study is to investigate the time-stress-humidity dependent behaviour of elementary hemp fibres. It proposes an experimental approach, using creep test at different constant load and relative humidity (RH) levels and also under cyclic-humidity and cyclic-load conditions. To investigate these topics, and particularly to ensure that the measurements are free of the uncertainties which arise from the strong variations in creep response occurring when a set of fibres is used, as previously observed (see Part I of this work), a deterministic

approach, with measurements *in situ* on a same, unique fibre is preferred in this part of the work.

MATERIALS AND METHODS

Water sorption isotherms and determination of water uptake

Isotherms of vapour water desorption/sorption were realized with a Dynamic Vapour Sorption (DVS) from Hiden Isochema Ltd. (UK). Measurements were performed on a set of isolated fibres with diameters varying between approximately 10 μm and 100 μm. This set is composed of both primary and secondary bast fibres and of elementary fibres and bundle of a few elementary fibres. Technical fibres were procured from the LCDA Company in a jumble state. The extraction of the fibres was processed using an immersion bath in water for 72h at 30°C.

The isolated hemp fibres (approx. 2.5 mg) were put into the inox nacelle of the microbalance (accuracy of 0.1 μg) and placed hermetically in the double jacket reactor connected to a thermostated water bath. The reactor was equipped with temperature and RH sensors to monitor these parameters (T° = 20°C). Relative humidity was obtained with the mix of wet and dry nitrogen flows. (Relative Humidity, accuracy 2%). A sequence of water sorption (10–90% at 10% intervals) and desorption (90–15 % at 15% intervals) was programmed. Equilibrium was detected by comparing the mass of sample with a mathematical asymptote model. When the difference was less than 1%, then the mass was noted. The dry hemp mass m_{dry} was obtained after the application of a drying sequence under a dry flow of nitrogen (240 min at 40 ◦C, then 480 min at 20 ◦C) corresponding to the 0% RH point. The hemp fibre water uptake ω was recorded at equilibrium for the chosen RH values and is calculated as following using the mass m_{moist} measured at the Equilibrium Moisture Content (EMC):

$$\omega(\%) = 100 \times \frac{m_{moist} - m_{dry}}{m_{dry}} \quad (1)$$

Tensile creep test on elementary fibre

The experimental methods and apparatus used for this study are widely described in this first part of this work (Part I). Only a change in the environmental chamber dimensions was performed in order to ensure a RH variation rate from 1%/min to 25%/min.

Single isolated hemp fibres were subjected to static and varying loads and varying climate conditions. The clamping length was 10 mm. The fibre elongation was measured and the strain calculated as the elongation divided by the initial fibre length. Tests were performed on fibres with an average external diameter of approximately 30 μm. The effective cross-section was determined using this mean external diameter assuming the fibre to be perfectly cylindrical and neglecting the lumen area. The stress was calculated using the applied force and the evaluated initial cross-section mean value of the fibre.

For each type of test, results are presented for only one single fibre. Three replicates were used to confirm the results we present here. The RH was controlled inside the sample chamber between 10% and 85% of RH.

Creep curve fitting

The creep functions recorded during tests were fitted using the anisotropic model and the fitting procedure (hybrid optimisation algorithm) described in the first part of the paper (Part I).

RESULTS AND DISCUSSION

Influence of loading on the creep behaviour

Loading level

Fig. 1 shows the evolution of the fibre strain at various increasing stress plateau and at constant temperature and humidity. The tested fibre presents a Type III' behaviour, as defined in the first part of this work (Part I). For the record, three main creep behaviours were observed. Type II is truly linear as a function of the logarithm of time while Type I and Type III are strongly nonlinear and can be described respectively by concave and convex functions. Tab. 1 provides a summary of the values of the instantaneous and time-delayed strains for each stress level. As expected, the instantaneous strain is most important for the first stress levels and decreases for the higher stress levels. This is consistent with the highly nonlinear

behaviour of most of the hemp fibres. As explained in a previous publication (*1*), an apparent decrease in rigidity is observed generally between 30 and 80 MPa (i.e. between the inflection points i_1 and i_2), and an increase in the fibre rigidity occurs for higher stress (Fig. 2). The apparent softening, in the first part of the stress-strain curve, was attributed to the reorganisation of the amorphous components and the hardening, in the last part of the curve, to a re-orientation of the cellulose microfibrils in the fibre direction and to a stress-induced crystallisation. The stiffening level is approximately 1.62 (from 26.5 GPa to 43 GPa) for a total axial strain of 2.1% (Tab. 1 and Fig. 1a), which is in a good agreement with previous results.

Single hemp fibres exhibit also a significant time-delayed behaviour which is widely influenced by the stress level (Fig. 1b, 1c and Tab. 1). After 10 000 s of tensile creep, the time-delayed strain reaches a value of 1 to 2.5 higher than the instantaneous strain as a function of stress level. The maximum value (0.39 %) is observed for a stress of 100 MPa.

For loading levels above 100 MPa (stress plateau 3, 4 and 5), and for the considered creep duration, the time-delayed strain decreases with the stress level (Tab. 1). The initial primary creep rate also decreases with increasing stress (Tab. 1). For these loading levels, the decrease in MFA (meaning that the microfibrils are more aligned in the longitudinal direction of the fibre) makes the expression of the cellulose microfibrils (highly crystalline and elastic) dominant on the amorphous matrix in the longitudinal direction. The part of viscosity in the global response of the fibre tends to decrease. Microfibrils re-orientation is certainly allowed by the breakage of inter-molecular linkages between the amorphous constitutive components of the cell wall and the cellulose microfibrils. When linkages break, additional creep movements could occur between macromolecular chains. This explains the increase in time-delayed strain for a stress of approximately 100 MPa. This decrease in viscosity is also consistent with the hypothetical stress-induced crystallisation of the paracrystalline cellulose [1]. For the lower loading levels, the viscoelastic behaviour could be attributed to the amorphous components of the cell wall.

In addition to the amplitude of both instantaneous and time-delayed strains, the shape of the creep function is also influenced by the stress level. As expected, and for each stress level, in the initial stage, the time-delayed strain rate decelerates with increasing time (Fig. 1b, Fig. 3). Under a constant stress of 50 MPa, the creep strain rate decreases from $2.47\ 10^{-5}\ s^{-1}$ to $3\ 10^{-8}\ s^{-1}$ between 10 and 10 000 s. Tab.1 gives the strain rate for the initial primary creep and the

secondary creep (at 10 000 s) for the different stress levels. This decrease in creep rate as a function of time slows with increasing stress (Fig. 3). It varies only from 0.25 10^{-5} s^{-1} to 1.25 10^{-7} s^{-1} at 250 MPa. So, this slowdown is varying from a factor 1000 at low stress level to a factor of only 20 at the highest stress level. This reflects a significant difference in the relaxation times.

Thus, single hemp fibres show highly nonlinear viscoelastic behaviour (the creep function directly depends on the loading stress). On the basis of the experimental results and more precisely of the creep functions under the different loading conditions, it was found very difficult to calibrate a nonlinear formulation, i.e. a time-stress equivalence.

To facilitate their description and their use, the creep functions recorded during tests were also fitted using the anisotropic model and the fitting procedure (hybrid minimisation algorithm) described in the first part of the paper (Part I). Fig. 4a shows 50 numerical curves obtained after launching the hybrid algorithm 50 times for the experimental test under a constant load of 50 MPa. The numerical results are clearly in a really good agreement with the experimental one. Fig. 4b presents the corresponding Inverse Gaussian (IG) spectrum obtained. The shape of the spectrum is consistent with the results obtained in the first part of this work (Part I) a Type III'curve, i.e. an IG spectrum with a truncation at the left side. This figure shows a large scattering in the IG spectrum as a function of the set number. This underlines the typical difficulty of the identification of complex behaviour models with restricted quantity of experimental data. In our work, only the axial compliance function has been determined experimentally. Under such conditions, the optimisation problem of minimizing the error between the experimental results and the model responses is multimodal and has multiple parameter sets. The overall properties of plant fibres (*13*), and specifically the tensile properties in our case are well-known to be highly scattered (*14, 15*). This is mainly attributed both to the biological origin of the material and to the experimental procedure. For time-dependent properties or other mechanical properties which required the use of a model to be identified, the parameters identification procedure can also contribute significantly to this scattering especially when the quantity of experimental data is restricted.

In this work, we proposed to discriminate a unique solution using the topology of the residual value of the objective function. Effectively, even if all the parameter sets are acceptable when performing a visual comparison between experimental and numerical curves (see Fig. 4a), several domains of solution, which are not equivalent in terms of error, can be identified depending on the topology. Fig. 4c and 4d reveal for this example 3 distinct domains of

response (Δ1, Δ2 and Δ3). These figures plot the residual value of the objective function (also called "error" later in this paper for reason of simplicity) as a function of respectively the set parameters number and the value of τ_1. In Fig. 4c, the sets are represented in ascending order of error value in order to facilitate the reading of the figure. Each domain of response is characterised by a specific value of error: Δ1 contains 7 sets with an error of approximately 2 10^{-6}, Δ2 35 sets with an error of 1.35 10^{-6} and Δ3 8 sets with an error of 6 10^{-7}. The scattering of the parameters inside each group is really different. While the inverse Gaussian spectrum are superimposed for the 8 sets included in Δ3, the spectrum contained in Δ2 and Δ1 are characterised by a large discrepancy in their shape and amplitude parameters (amplitude, time constant and truncation). This is particularly true for τ_1 (see Fig. 4d). So, the topology of the objective function reveals not only a multi-modal solution, but also different accuracy for these solutions. In this study, we propose to discriminate the best solution using this topology (see Fig. 4c and 4d, red dotted-line). For this experimental curve, the selected solution is defined by the Δ3 domain and is characterised by the lowest error between experimental and numerical curves and an insignificant scattering in parameters values (coefficient of variation lower than 10^{-4}).

The methodology was applied for each experimental curve collected at the different stress plateau. Fig.5 shows the error vs. set number for each stress plateau. The error level varies between 10^{-7} and 10^{-6} and the population of the Δ3 domain includes 3 to 8 draws (from a total number of 50) as a function of the experimental curve. This level depends mainly on the signal to noise ratio of the experimental curve. The small number of individuals in the Δ3 domain also demonstrates the difficulty to detect the zone of interest in the parameter space and underlines the need to use metaheuristic models to ensure reliable parameter identification in such context.

Fig. 6 shows the IG spectrum identified at each stress level (Δ3) and Tab. 2 synthetises the values of the identified parameters. The influence of stress level on the values of the identified axial component of the viscoelastic compliance (S_{ZZ}) and of the time constant τ_1 is significant. S_{ZZ} is found to decrease as a function of increasing stress, varying from 4.2 10^{-5} to 1.2 10^{-5} MPa^{-1} between 50 MPa and 250 MPa. Such empirical relationship could be used to calibrate a time-stress equivalence.

Cyclic-load creep

Two types of constant/cyclic-load creep were performed. For the first experiment, a stress of approximately 40 MPa (below the yield point i_1) was applied for 7000 sec. Then, the load was cycled between 10 and 40 MPa. After ten cycles, the load was returned to its original value and the creep experiment was continued. For the second one, after the first stage, the load was cycled between 30 and 115 MPa. After four cycles, the load was maintained to this maximum value and the creep experiment was continued (Fig. 7).

Results are presented in Fig. 7. In the first case, the cyclic-load creep rate is of the same order of magnitude that the constant-load creep one (Fig. 7a). After load cycling, the constant-load creep rate still remains constant.

In the second case (Fig. 7b), when cyclic load excursions overpasses the constant average load, we can notice that load cycling greatly increases the average creep rate (from $5.8\ 10^{-7}\ s^{-1}$ to $4.8\ 10^{-6}\ s^{-1}$) and produces a large injection of extra creep strain. The maximum load excursion (115 MPa) could overpass the yield point i_1 and then express the inelastic mechanisms involved in the nonlinear tensile behaviour of the fibres (see Fig. 2)

After load cycling, the constant-load creep strain rate was greatly reduced ($8.4\ 10^{-8}\ s^{-1}$). This result was also observed by Haberger et al. [4] on Kevlar fibre.

Influence of moisture on the creep behaviour

Moisture level

Measurements were made at different constant humidity levels, kept at 20, 40, 60 and 80% which correspond to approximately 5.5%, 8%, 10.5% and 15.5%, respectively in terms of EMC based on the sorption/desorption isotherm of isolated hemp fibres (Fig. 8). As expected and as observed for many lignocellulosic materials, the adsorption/desorption properties of isolated hemp fibres are characterized by a sigmoidal shaped of the isotherms and hysteresis between the sorption and desorption loops. This shape results from the combination and the competition of the different involved sorption mechanisms and their kinetic (*16, 17*). The time to reach the moisture content equilibrium when submitted to a change in RH depends on the accessibility of the sorption sites and on the size of the fibre (and more exactly of the thickness of the cell wall). Fig. 9 shows the mass change (i.e. water adsorption) over time profile of the full sorption cycle for isolated hemp fibres at 20°C. The time to reach the equilibrium is dependent on the RH level. To reach 90% of the EMC, 14 min to 23 min are required (Tab. 3). Tab. 3 also shows that more than 75% of the EMC is reached after 10 min

of water vapour sorption. These measurements were performed on a set of isolated fibres and bundles. It can be considered that the time to reach the equilibrium at the unitarian fibre scale is lower. In our work, 10 to 15 min of pause time was observed before starting the mechanical loading to let the fibre attains its moisture content equilibrium.

The moisture uptake also causes a swelling of the fibres, which is a dimensional change due to breaking of inter and intramolecular hydrogen bonds between the macromolecules. In this work, due to experimental difficulties, the cross-section variation, induced both by the mechanical loading and the vapour water sorption, was not taken into to account. It is also important to notice that the moisture uptake in the wall can vary according to the stress applied to the fibre (*18*) and also as a function of the degree of crystallinity.

The interfibre variation in creep behaviour is quite large (see Part I) and the investigation of the influence of humidity on the creep behaviour is particularly difficult when using stochastic approach. As for quasi-static tensile tests (*2*), we preferred a deterministic approach based on a same fibre. Replicates were used to confirm the results we present here.

Fig.10 shows the evolution of the axial strain as a function of time when the fibre is submitted to a constant axial load and to successive incremental RH plateau (20% to 80% with 20% intervals). Significant additional strains are observed at each RH increase, indicating the existence of mechanosorptive phenomena. Again, the strain rate is high in the first stage following the RH variation and slows as a function of time. The amplitude of this water sorption induced strain is particularly important when the RH is changing from 60% to 80%. This could be explained by the higher jump in moisture content (approximately 5%) obtained on this RH step in comparison to the approximately 2% observed for the other RH steps. Beyond this limit (60-70% in RH, see the inflection point on the sorption isotherm, Fig. 8), a saturation of the hydroxyl groups is generally observed for cellulosic materials, and the water absorption can induce an increase in the free volume between macromolecules in the amorphous components and consequently in the molecule mobility.

These additional strains measured when water content increases in fibre could result from a change both in elastic and inelastic properties of the fibre. In a previous work, we observe a great influence of humidity on the apparent rigidity of such fibres (*2*).Using this type of experimental protocol, elastic and inelastic contributions cannot be deconvoluted. To achieve it, we propose to perform several creep/recovery tests on a same single fibre at increasing RH levels. Results are presented in Fig. 11. Creep properties are synthesized in Tab. 4. If the instantaneous strain is not significantly affected by the RH level, it clearly appears that the

time-delayed strain considerably increases with increasing RH (Fig. 11b and Tab. 4). For the considered creep time (4000 s), the time-delayed strain is of about 0.19% at 40% RH and 0.63% at 80% RH. Both primary creep and secondary creep rates also increase with RH. Between 40% and 80% RH these rates are respectively multiplied by factors 5 and 7 (Tab. 4). Humidity is clearly an activator of the viscoelastic properties of hemp fibres. This is confirmed by the parameters of the viscoelastic model which were identified at each RH level. Fig. 12 shows the IG spectrum identified at each stress level and Tab. 5 synthetises the values of the identified parameters. RH increase induces an increase in S_{ZZ} and $\tau_1$values. It varies respectively from 4.7 10^{-5} to 1.5 10^{-4} MPa^{-1} and from approximately 19 s to 92 s between 40% and 80% of RH. Again, such empirical relationship could be used to calibrate a time-humidity equivalence.

Creep under cyclic humidity conditions: mechanosorptive effect

Two types of constant/cyclic-humidity creep were performed. For the first experiment, a RH of approximately 80% was applied for 8000 s. Then, the RH was cycled between 80 and 15% at a RH variation rate of 8%RH.min^{-1}. After five cycles, the RH was returned to its original value and maintained constant for a few hours. Throughout the test, the tensile load is constant and corresponds to an initial tensile stress of 50 MPa. For the second one, after the first stage, the RH was cycled at a RH variation rate of 20%RH.min^{-1}.

Fig.13 shows the evolution of the creep strain of the two tested fibres as a function of time. As expected, the strain decreases and increases respectively when the fibre is submitted to drying and wetting. These variations in strain are attributed to the dimensional changes induced by water sorption and also by the change in mechanical properties (both elastic and viscoelastic). In the first case, the average cyclic-RH creep rate is of the same order of magnitude that the constant-RH creep one (Fig. 13a). After RH cycling, the constant-RH creep rate still remains constant. In the second case (Fig. 13b), we can notice that the average cyclic-RH creep rate is higher than the constant RH-creep rate. This phenomenon is generally called mechanosorptive creep. This result is in agreement with the work of Haberger *et al*. (*7*) who have observed for several hydrophilic fibres that the MCS creep occurrence is dependent on the moisture cycling rate. The time parameters of the humidity cycling must be matched to the sorption time of the sample, and therefore to the size of the fibre and of the wall thickness. For low RH rates, this match is not respected and the creep is not accelerated. This observation also supports the

sorption-induced stress-gradient explanations proposed by these authors. In a previous work (*19*), we showed that when considering that the fibre has a constant and cylindrical cross-section along its length and using a theoretical model, an axial stress gradient is established across the fibre wall under tensile loading. The axial stress is the highest at the inner face of the cell wall and progressively decreases with the thickness of the cell wall. When the fibre is submitted to a quick variation in RH, it starts to dry (or wet) from the outside. The outer parts of the fibre respond by shrinking (swelling) and changing their elastic properties. This could induce additional axial stresses which are redistributed across the sample (Fig. 14). The change in mechanical properties can also be heterogeneous as a function of the wall sub-layers (and their biochemical composition), which could also emphasize the axial stress gradient. Successive sorption and desorption cycles consequently induce cyclic loading with high-stress excursion (over-passing the average stress level). As previously observed in this work (see Fig. 7b), load cycling greatly increases the average creep rate and produces a large injection of extra creep strain when the cycling load overpasses the constant-load. The additional creep strains accumulated during the high-stress excursions makes that the creep is greater on cyclic loading than at a constant average stress.

The two RH cycling rates (8 and 20%RH.min^{-1}) were tested on two different fibres (Fig. 13). To confirm that the observed accelerated creep is due to RH cycling and not to inter-fibre variability, the two RH cycling parameters were tested on a same fibre (Fig. 15). A RH of approximately 80% was applied for 5000 s. Then, the RH was cycled between 80 and 15% at a RH variation rate of 20%RH.min^{-1}. After five cycles, the RH was returned to its original value and maintained constant for 5000s. The RH was again cycled between 80 and 15% but for this sequence at a RH variation rate of 8%RH.min^{-1}. After five cycles, the RH was again returned to its original value and maintained constant for 5000s. A considerable acceleration in creep strain rate (5.5 10^{-8} s^{-1} to 2.7 10^{-7} s^{-1}) is observed when the first RH cycling stage is applied. When the RH is returned to its maximal and constant value, the creep strain rate decreases to reach a value in the same order of magnitude that the initial one (3 10^{-8} s^{-1}). This rate remains constant during the second RH cycling stage (with the low RH rate) and during the successive RH plateau. This confirms that the creep acceleration under cyclic RH is only observed for high RH rates.

CONCLUSION

Results showed a time-stress-humidity dependent behaviour of hemp fibres. The stress level significantly influences the creep behaviour. Both instantaneous and time-delayed strains decrease with increasing stress above the yield point i_1. Load cycling at an average load higher than constant creep load produces a large injection of extra creep strain and an increase in the creep strain rate.

Tensile creep is also highly influenced by RH level and variation. The time-delayed strain considerably increases with increasing moisture content. Creep rate under cyclic humidity conditions exceeds any constant creep rate if the rate of cyclic RH variation overpasses 10 % RH/min for hemp fibres of about 30 μm in diameter. If the question of the origin of this mechanosorptive mechanism remains open, our result seems to be consistent with sorption-induced stress-gradient explanations.

ACKNOLEDGEMENTS

The authors would like to thank Camille Garcin from the FEMTO-ST for his assistance with some of the experiments.

REFERENCES

1. Placet V, Cisse O, Boubakar L (2014) Nonlinear tensile behaviour of elementary hemp fibres. Part I: Investigation of the possible origins using repeated progressive loading with in situ microscopic observations. Composites Part A: Applied Science and Manufacturing 56:319
2. Placet V, Cisse O, Boubakar ML (2012) Influence of environmental relative humidity on the tensile and rotational behaviour of hemp fibres. Journal of Materials Science 47 (7):3435
3. Navi P, Stanzl-Tschegg S (2008) Micromechanics of creep and relaxation of wood. A review COST Action E35 2004–2008: Wood machining – micromechanics and fracture. Holzforschung 63(2):186
4. Sedlachek K, Ellis R (1994) The effect of cyclic humidity on the creep of single fibers of Southern pine. In: Fellers C LT, ed. Moisture-induced creep behaviour of paper and board. Stockholm: STFI, USDA, 1994:22.
5. Sedlachek K (1995) The effect of hemicelluloses and cyclic humidity on the creep of single fibres. Inst Paper Sci Technol: Georgia Tech.
6. Coffin D, Boese S (1997) Tensile creep behavior of single fibers and paper in a cyclic humidity environment. 3rd Int. Symp. On Moisture and Creep effects on paper and containers. Rotorua, New-Zealand.
7. Haberger C, Coffin D, Hojjatie B (2001) Influence of humidity cycling parameters on the moisture-accelerated creep of polymeric fibers. J Polym Sci Pol Phys 39:2048

8. Dong F, Olsson A-M, Salmén L (2010) Fibre morphological effects on mechano-sorptive creep. Wood Science and Technology 44 (3):475

9. Olsson A-M, Salmén L, Eder M, Burgert I (2007) Mechano-sorptive creep in wood fibres. Wood Science and Technology 41(1):59

10. Olsson A-M, Salmén L (2014) Mechano-sorptive creep in pulp fibres and paper. Wood Science and Technology 48 (3):569

11. Haberger C, Coffin D (2000) The role of stress concentrations in accelerated creep and sorption-induced physical aging. J Pulp Pap Sci 26(4):145

12. Lindström S, Karabulut E, Kulachenko A, Sehaqui H, Wagberg L (2012) Mechanosorptive creep in nanocellulose materials. Cellulose 19(3):809

13. Beaugrand J, Nottez M, Konnerth J, Bourmaud A (2014) Multi-scale analysis of the structure and mechanical performance of woody hemp core and the dependence on the sampling location. Industrial Crops and Products 60(0):193

14. Shah D (2013) Developing plant fibre composites for structural applications by optimising composite parameters: a critical review. Journal of Materials Science 48(18):6083

15. Summerscales J, Dissanayake NPJ, Virk AS, Hall W (2010) A review of bast fibres and their composites. Part 1- Fibres as reinforcements. Composites Part A: Applied Science and Manufacturing 41(10):1329

16. Hill CAS, Norton A, Newman G (2009) The water vapor sorption behavior of natural fibers. Journal of Applied Polymer Science 112(3):1524

17. Bessadok A, Langevin D, Gouanvé F, Chappey C, Roudesli S, Marais S (2009) Study of water sorption on modified Agave fibres. Carbohydrate Polymers 76(1):74

18. Bertinetti L, Fischer FD, Fratzl P (2013) Physicochemical Basis for Water-Actuated Movement and Stress Generation in Nonliving Plant Tissues. Physical Review Letters 111(23):238001

19. Trivaudey F, Placet V, Guicheret-Retel V, Boubakar L (2014) Nonlinear tensile behaviour of elementary hemp fibres. Part II: Modelling using an anisotropic viscoelastic constitutive law in a material rotating frame. Composites Part A: Applied Science and Manufacturing, In Press.

a.

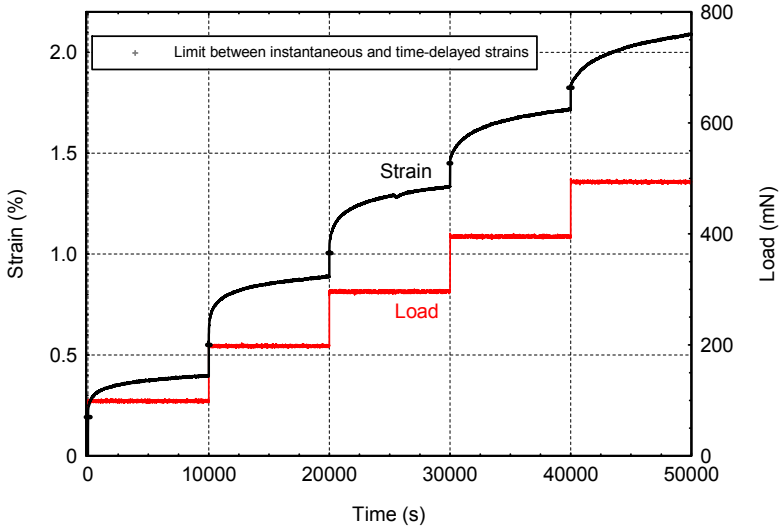

b.

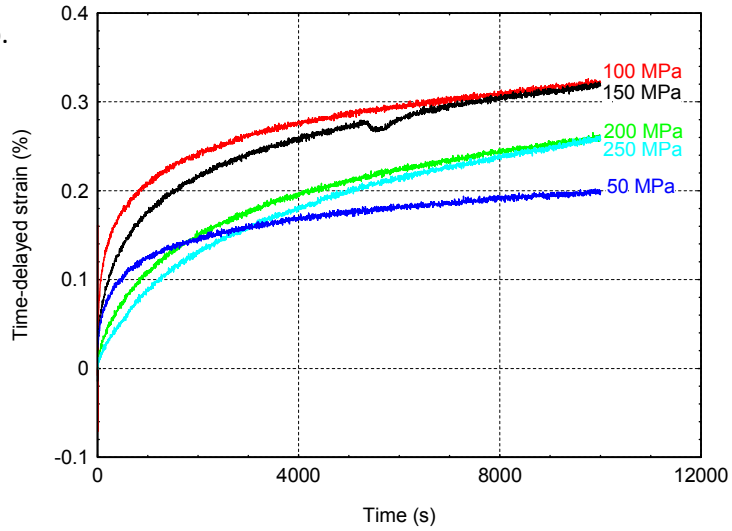

c.

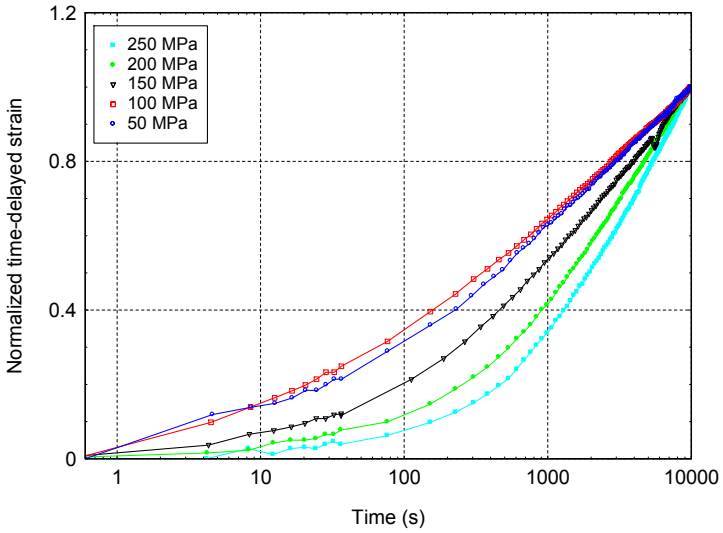

Figure 1 : Creep behaviour under increasing stress plateau up to rupture (T=23°C ±1.5°C, RH=50% ±2.5%). a. Strain and load as a function of time. b. Time-delayed strain as a function of time for each stress level. c. Normalized time-delayed strain as a function of the logarithm of time.

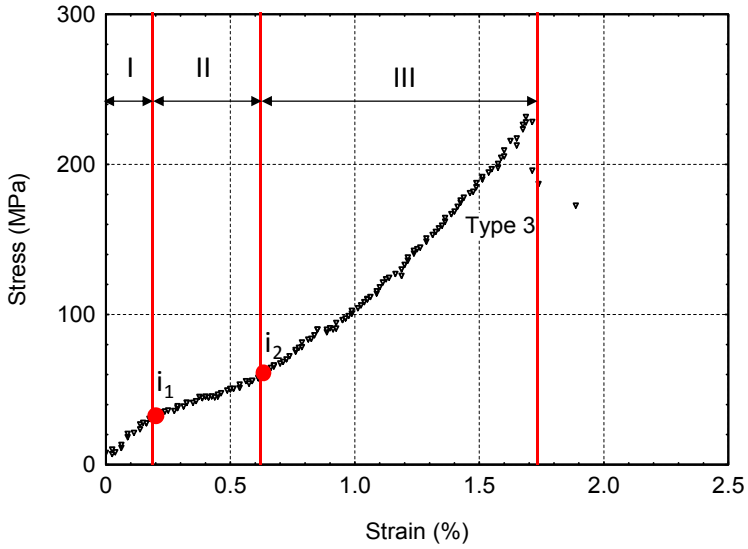

Figure 2 : Typical stress-strain curve of single hemp fibre under tensile test, from Placet et al. (*1*).

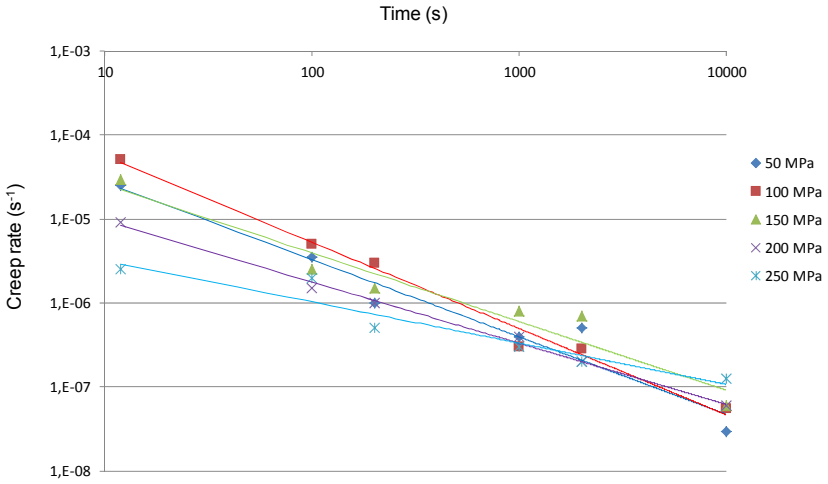

Figure 3 : Evolution of the creep rate as a function of time for each constant stress level.

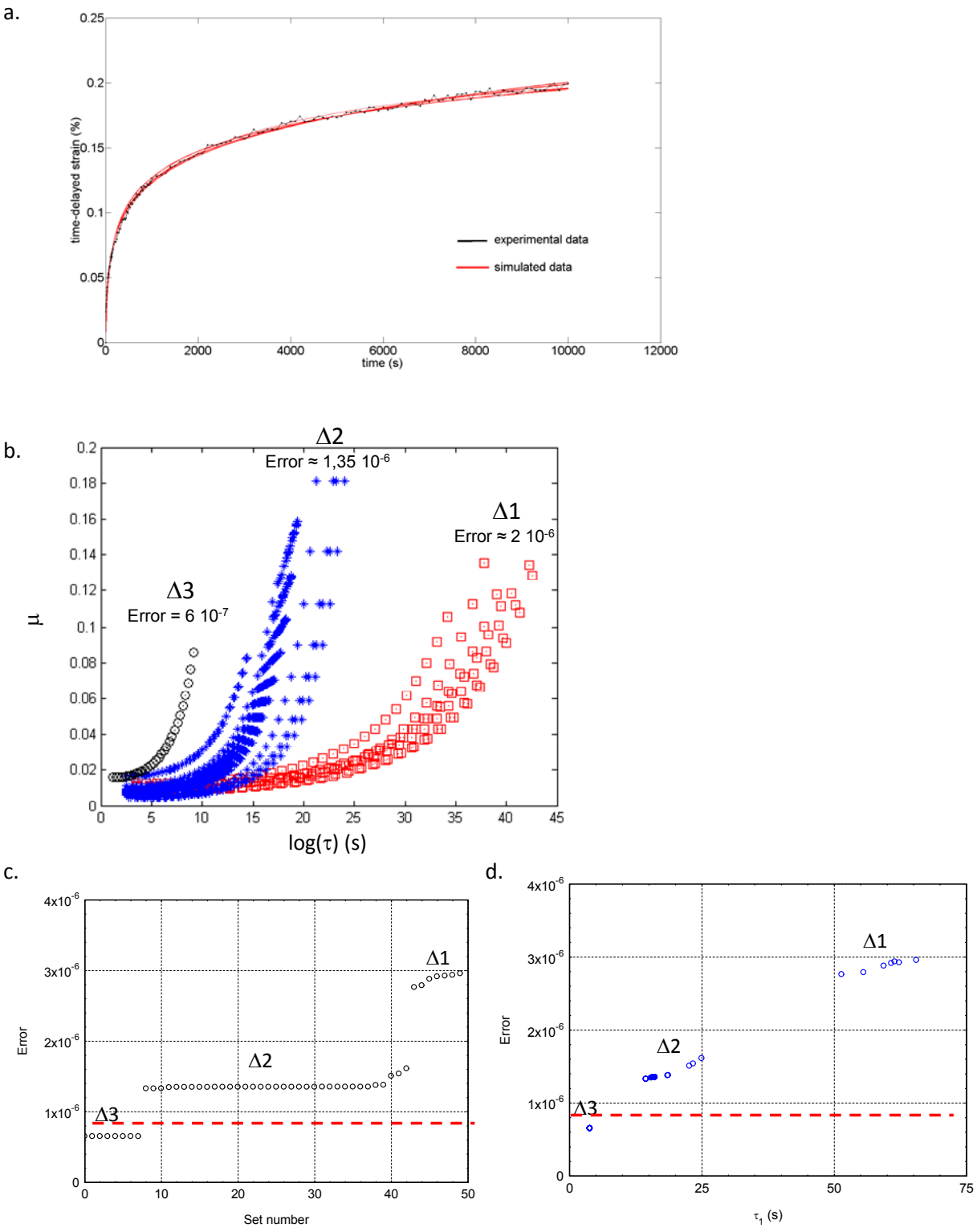

Figure 4 : a. Comparison between an experimental curve (constant load 50 MPa) and 50 numerical curves identified using the proposed model and identification method. b Inverse Gaussian distribution functions for the 50 identified sets. c. Error between the experimental curve and each numerical curve as a function of the set number. d. Error as a function of the identified value of the parameter τ_1.

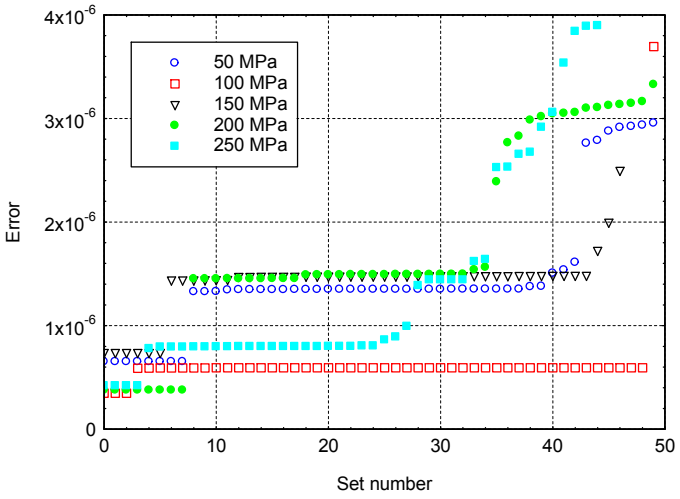

Figure 5 : Error between the experimental and numerical curves as a function of the set number for each stress level creep function.

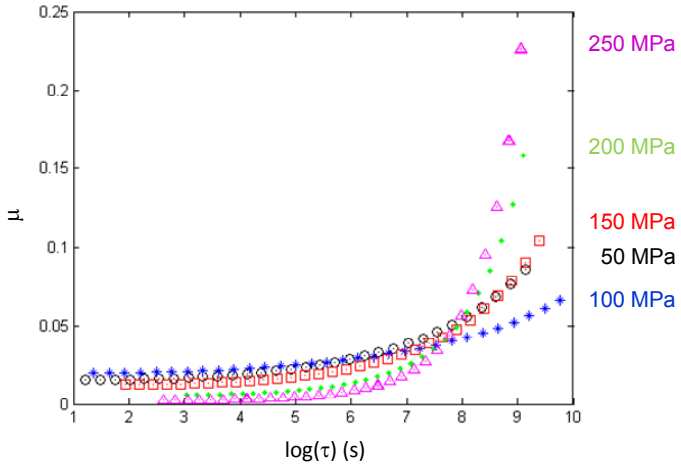

Figure 6 : Inverse Gaussian distribution functions identified for each stress level creep function

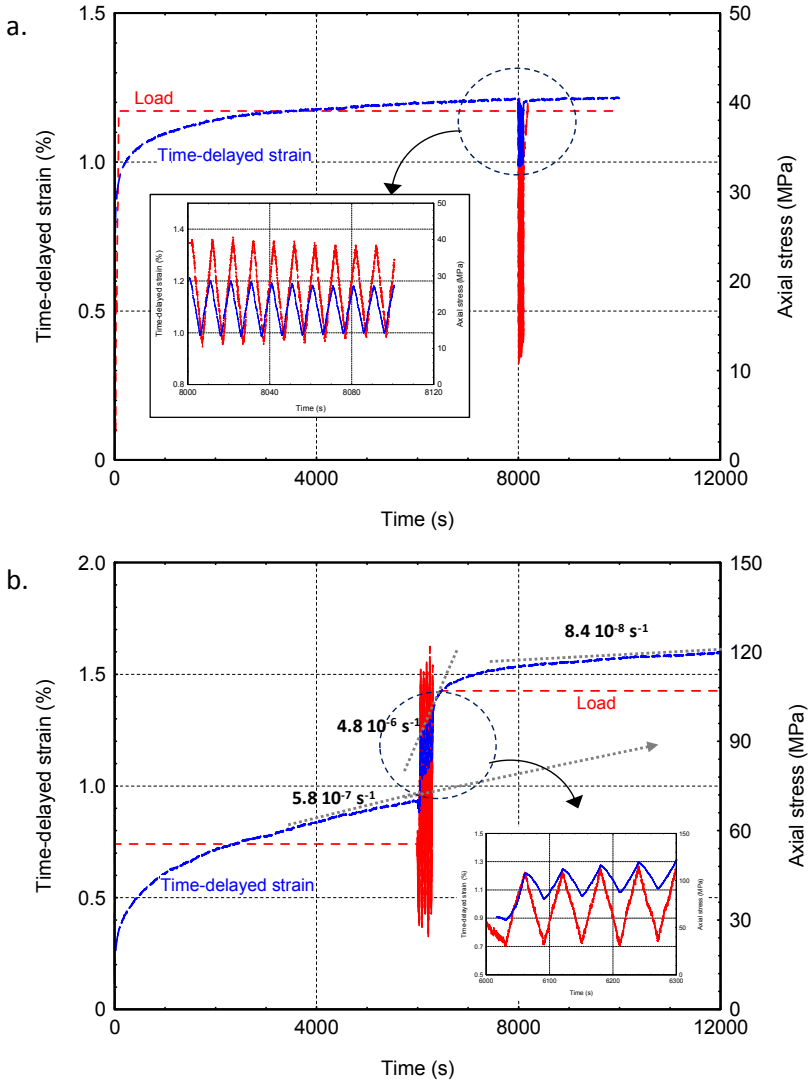

Figure 7 : Evolution of the fibre strain at constant relative humidity and constant/cyclic load (T=23°C ±1.5°C, RH=50% ±2.5%). a. Cyclic loading between 10 and 40 MPa. b. Cyclic loading between 30 and 115 MPa

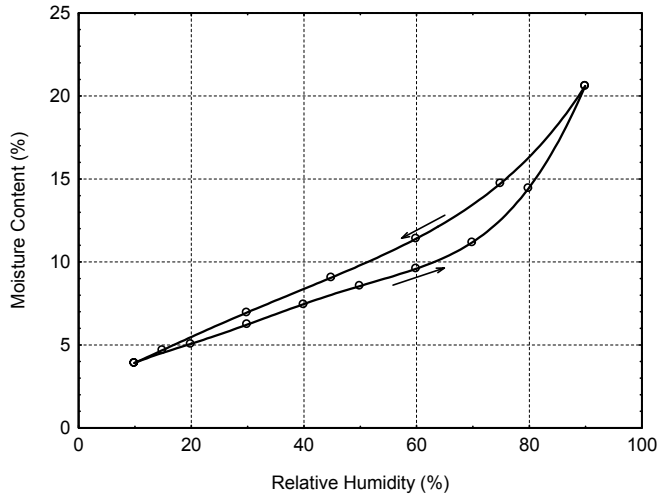

Figure 8 : Equilibrium moisture sorption and desorption isotherms of isolated hemp fibres and bundles at 20°C.

a.

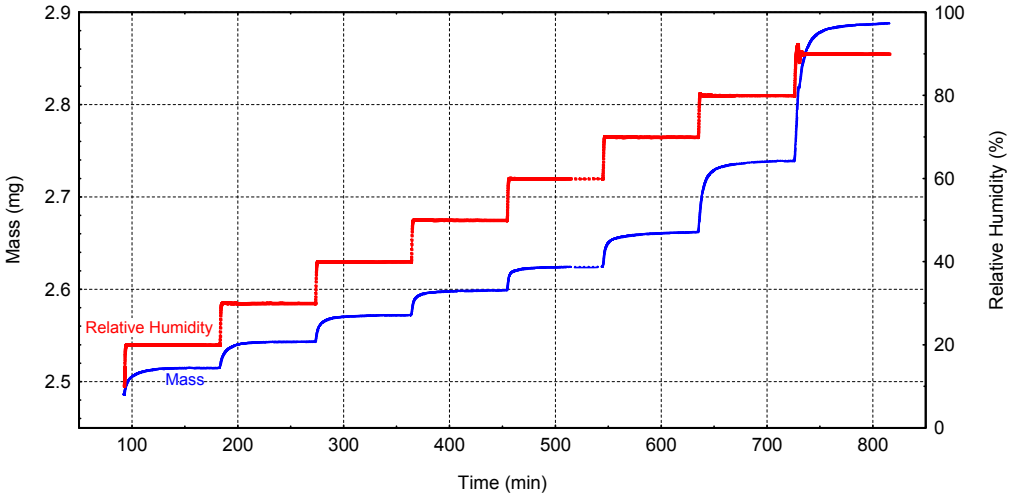

b.

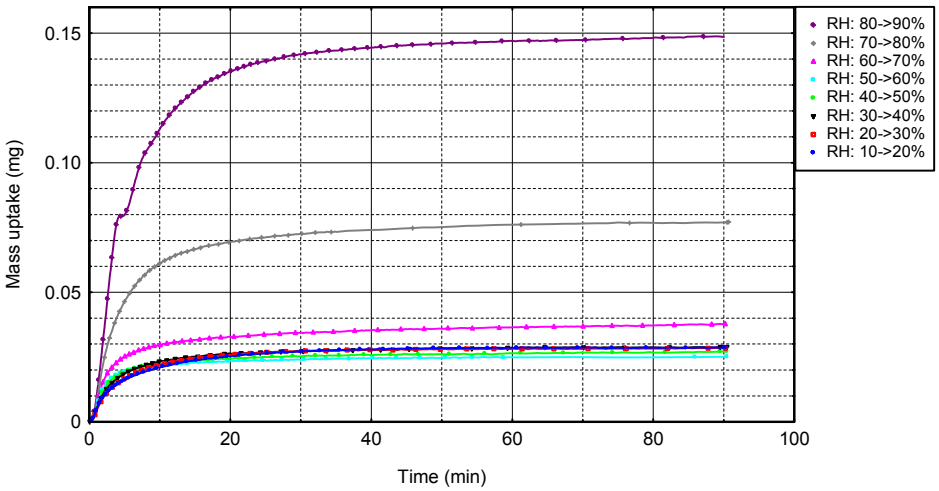

Figure 9 : Mass change over time profile of sorption cycle for isolated hemp fibres and bundles at 20°C. a. Full sorption cycle. b. Sorption curves at each RH step superimposed after time re-zeroing.

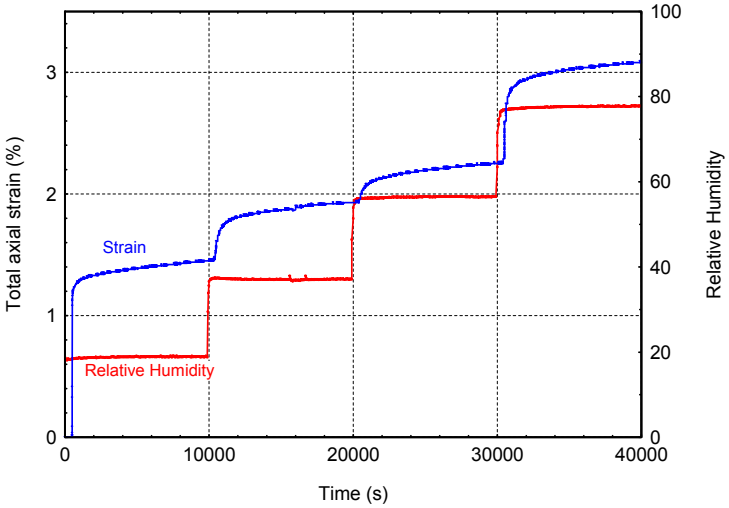

Figure 10 : Evolution of strain as a function of time for a single fibre under constant load (corresponding to an initial tensile stress of 50 MPa) at different RH plateau: 20, 40, 60 and 80% RH (T=23°C ±1.5°C).

a.

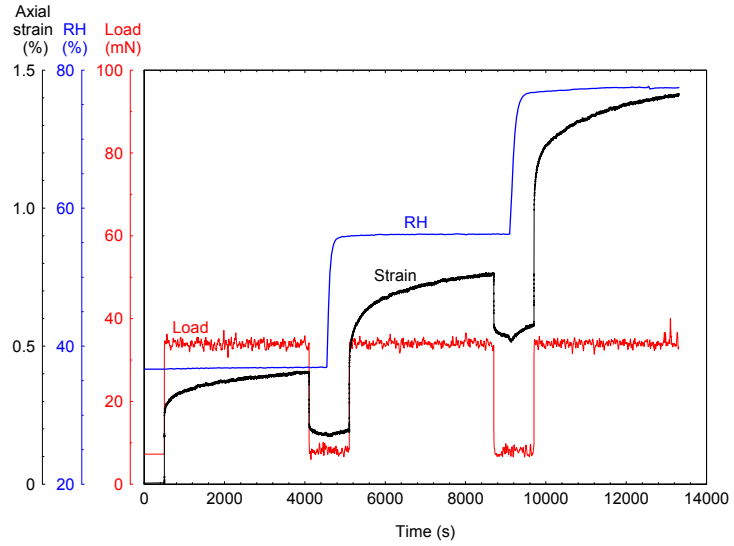

b.

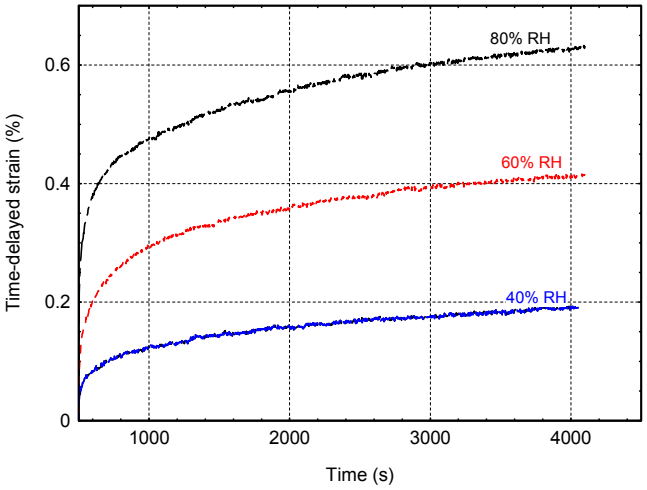

Figure 11 : Successive creep/recovery tests on a same single fibre at increasing RH levels: 40, 60 and 80% RH (T=23°C ±1.5°C). a. Full experiment. b. Superimposed creep curves recorded at each successive RH plateau after time re-zeroing.

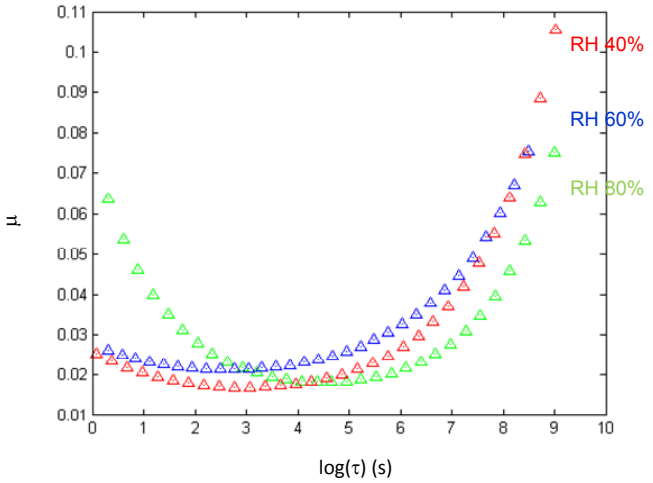

Figure 12 : Inverse Gaussian distribution functions identified for each RH level creep function

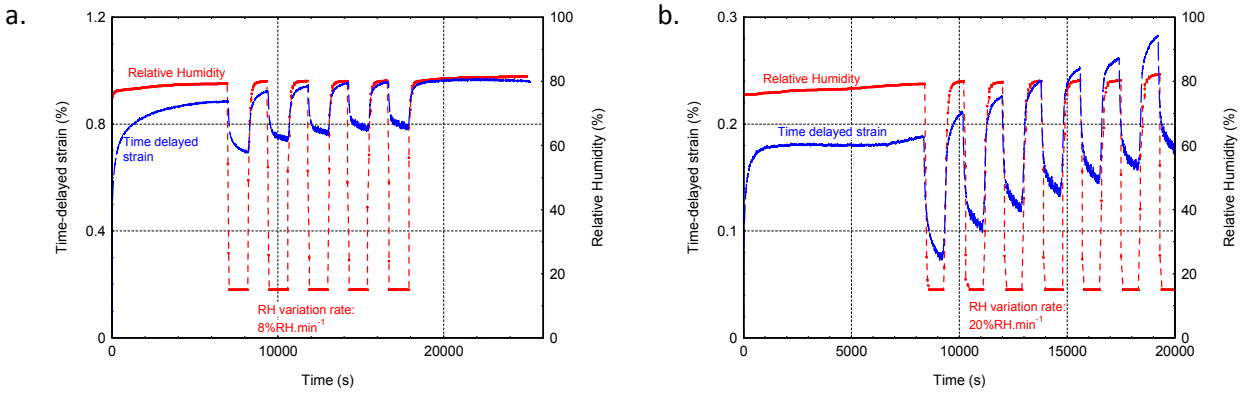

Figure 13 : Evolution of creep strain of single hemp fibres as a function of time for varying RH between 15% and 80%. a. RH variation rate = 8%RH/min. b. RH variation rate = 20%RH/min. Initial constant tensile stress = 50 MPa, T = 25°C±1.5°C.

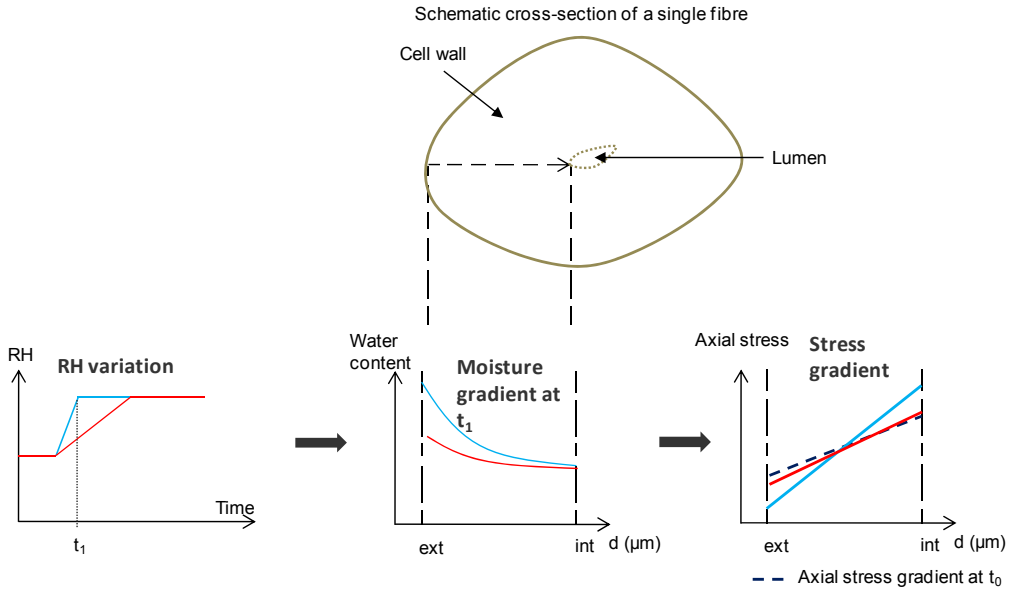

Figure 14 : Schematic representation of the sorption-induced stress gradient in the fibre wall and its possible influence of the mechanosorptive creep.

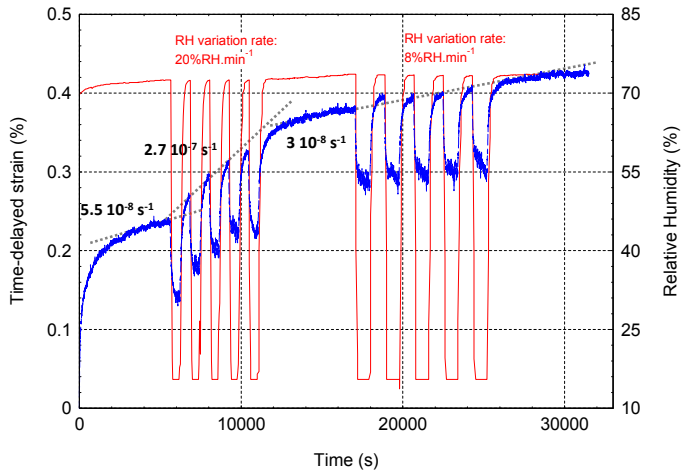

Figure 15 : Evolution of creep strain as a function of time for a single fibre submitted to two successive stages of RH cycling with a respective variation rate of 8%RH/min and 20%RH/min (Stress = 50 MPa, T = 25°C±1.5°C).

Table 1: Creep properties for a single hemp fibre submitted to constant loading at different stress levels.

Loading (mN)	Corresponding initial tensile stress (MPa)	Instantaneous apparent modulus (GPa)	Instantaneous-strain (%)	Time-delayed strain (%) after 3600 s	Time-delayed strain (%) after 10000 s	Initial primary creep strain rate 10^{-5} s^{-1}	Secondary creep strain rate 10^{-8} s^{-1}
100	50	26.5	0.192	0.165	0.200	2.45	3
200	100	32	0.163	0.276	0.388	5.1	5.5
300	150	37	0.125	0.254	0.319	2.9	6
400	200	41	0.124	0.188	0.257	0.9	6
500	250	43	0.117	0.174	0.262	0.25	12.5

Table 2: Fitted parameters for the different creep curves recorded at different stress levels for inverse Gaussian spectral model

Stress level (MPa)	τ_1 (s)	σ_d (s)	S_{ZZ} (MPa^{-1})	n_{min}	n_{max}
50	3.9	4.2	$4.2\ 10^{-5}$	0.01	0.61
100	4.6	5.4	$3.6\ 10^{-5}$	0.01	0.51
150	7.7	3.6	$2.4\ 10^{-5}$	0.01	0.68
200	22.2	2.4	$1.5\ 10^{-5}$	0.01	0.84
250	14.7	2.1	$1.2\ 10^{-5}$	0.01	0.99

Table 3 : Time to reach the Equilibrium Moisture Content when the fibres are submitted to vapour water sorption

RH step (%)	Time to reach 90% of the EMC (min)	Percentage of EMC reached after 10 min (%)
10->20	22.6	73
20->30	18.5	78
30->40	18.1	81
40->50	22.4	83
50->60	14	87
60->70	27	79
70->80	20.1	80
80->90	18.7	77
90->75	8.2	92
75->60	10.7	89
60->45	18.8	84
45->30	17.1	84
30->15	24.1	78

Table 4 : Creep properties for a single hemp fibre submitted to different dwells in RH (Constant stress: 50 MPa)

RH (%)	EMC (%)	Instantaneous strain (%)	Time-delayed strain (%)	Initial primary creep strain rate 10^{-5} s^{-1}	Secondary creep strain rate 10^{-8} s^{-1}
40	8	0.21	0.19	4.1	4
60	10.5	0.17	0.39	8.7	12.5
80	15.5	0.2	0.63	20.4	29.4

Table 5: Fitted parameters for the different creep curves recorded at different RH levels for inverse Gaussian spectral model

RH (%)	τ_1 (s)	σ_d (s)	S_{ZZ} (MPa^{-1})	n_{min}	n_{max}
40	19.3	3.2	$4.7\ 10^{-5}$	0.3	0.64
60	14.4	3.7	$9.2\ 10^{-5}$	0.21	0.53
80	92.1	2.7	$1.5\ 10^{-4}$	0.53	0.56